Available online at www.sciencedirect.com

SciVerse ScienceDirect

Ceramics International 38 (2012) 3625–3634

CERAMICS INTERNATIONAL

www.elsevier.com/locate/ceramint

Low temperature hydrothermal synthesis and characterization of Mn doped cobalt ferrite nanoparticles

Yüksel Köseoğlu [a,*], Furkan Alan [a], Muhammed Tan [a], Resul Yilgin [b], Mustafa Öztürk [b]

[a] Department of Physics, Fatih University, Buyukcekmece, 34500 İstanbul, Turkey

[b] Department of Physics, Gebze Institute of Technology, Cayirova, 41400 Kocaeli, Turkey

Received 21 October 2011; received in revised form 29 December 2011; accepted 1 January 2012

Available online 8 January 2012

Abstract

A series of Mn doped cobalt ferrite compounds with the formula $Mn_xCo_{1-x}Fe_2O_4$ where $x = 0.0$, 0.2, 0.4, 0.6, 0.8 and 1.0 were successfully synthesized by polyethylene glycol-assisted hydrothermal method. All samples were found to have cubic spinel structure. Average crystallite sizes of the nanoparticles were estimated using Debye–Scherrer's equation and found to be in between 14 and 22 nm with small size distribution. SEM was used to study morphological variations and EDX results showed that the compositional mass ratios were relevant as expected from the synthesis. VSM measurements show that all samples possess both ferromagnetic and superparamagnetic phases separated by blocking temperatures that decrease with increase in Mn content. Likewise, coercive fields and remanent magnetizations of the samples generally decrease as the parameter x goes from 0.0 to 1.0. They show ferromagnetic behaviors at temperatures lower than the blocking temperature. Magnetization and the coercive field of the samples increase by decreasing the temperature.

Keywords: Hydrothermal synthesis; XRD; VSM; SEM; Magnetic nanoparticles; Mn–Co spinel ferrites

1. Introduction

The magnetostrictive materials, having versatile application areas, have long been to be the subject of extensive research mainly due to the growing number of possible applications in technological, medical and industrial applications. Most technological and medical applications require nanoparticles (NPs) with smaller sizes and narrow size distribution to have uniform physical and chemical properties. Small size and large surface-to-volume ratio leads to distinct magnetic properties which are different from those of their bulk counterparts. This behavior has been explained as due to the large volume fractions of the atoms in the grain boundary area with unusual properties like spin canting, surface anisotropy, dislocations and superparamagnetic behavior [1–19]. In this context, nanosized spinel ferrite particles have also attracted considerable interest, and many efforts continue to investigate them for their technological applications in the microwave industries, magnetic recording, refrigeration systems, electrical devices, ferrofluids, MRI imaging, drug delivery, etc. [1–7]. Spinel structure generally allows the introduction of different metallic ions as dopants, which can change the magnetic and electrical properties considerably. Ferrites whose general structure is $[A^{2+}]_{tet}$ $[B^{3+}]_{octa}O_4$ are well known for their electrical, magnetic and catalytic properties [8–10]. In a spinel structured compound AB_2O_4 the unit cell contains 32 oxygen atoms in cubic close packing with 8 tetrahedral (A) and 16 octahedral (B) occupied sites. Magnetization of spinel ferrites originates from difference in the magnetic moments of the cations distributed at tetrahedral A and octahedral B sites and this depends on the superexchange interactions through oxygen as J_{AB} (A–O–B), J_{AA} (A–O–A) and J_{BB} (B–O–B). When J_{AB} is the strongest interaction, ferrimagnetism occurs. Among the ferrospinels, the inverse type is particularly interesting due to its high magneto-crystalline anisotropy, high saturation magnetization, and unique magnetic structure [11]. Manganese doped cobalt ferrites are promising ones for magnetic stress sensors, noncontact torque sensing, magnetoptical, magneto-mechanical, and high magnetostriction applications [12–15]. The magnetization in Mn doped cobalt ferrites is expected to

* Corresponding author. Tel.: +90 212 8663300; fax: +90 212 8663402.
E-mail address: yukselk@fatih.edu.tr (Y. Köseoğlu).

0272-8842/$36.00
doi:10.1016/j.ceramint.2012.01.001

depend on the cation distribution of the magnetic Fe^{3+}, Mn^{2+} and Co^{2+} ions among the A and B sites.

Cobalt ferrite, $CoFe_2O_4$, is a well-known hard magnetic material, which has been studied in detail due to its high coercivity (5400 Oe), high chemical stability, good electrical insulation, significant mechanical hardness and moderate saturation magnetization (*80 emu/g) at room temperature. However, in the case of nanosized $CoFe_2O_4$ particles, different values of coercivity and saturation magnetization have been reported [11,16–18]. The reason is that the magnetic properties of nanosized particles depend on the particle size and the preparation method. Coey [19] explained the reduction of saturation magnetization of nanosized ferrites by considering a spin configuration that differs from the Neel type found in large particles. He proposed that the spins are canted at the surface of the nanoparticles; i.e., the ions in the surface layer are inclined at various angles respect to the direction of the net moment. In this way, the particle magnetization cannot be seen as uniform through the nanoparticle and it is the result of a magnetic ordered core and a surrounding surface shell of disordered spins [5,10,19].

Agglomeration is one of the main constrains in the synthesis of magnetic nanoparticles and can be reduced by incorporating them in to a polymeric matrix or by using surfactant which covers the nanoparticles surfaces and decrease the agglomeration [10,21]. There are various methods to obtain magnetic nanoparticles among them hydrothermal method has low sintering temperature, low cost and need less energy.

To the best of our knowledge, only a few reports are available for the synthesis and magnetic behavior of Mn doped cobalt ferrite NPs. In this work, we prepared $Mn_xCo_{1-x}Fe_2O_4$ NPs with a low sintering temperature involving less energy and low-cost coating material (polyethylene-glycol (PEG)) by surfactant assisted hydrothermal method for the first time and detailed structural and magnetic characterizations of Mn doped cobalt ferrite nanoparticles are investigated. We used PEG as the surfactant which is one of the polymers with major interest in this area because it is non-toxic, non-flammable and easy to handle. Various morphologies with different sizes and shapes can be obtained by PEG-coating. It is verified that using PEG is very advantageous to prevent agglomerations and to obtain small particle sizes with good crystallinity as emphasized in different works [9,20–23].

2. Experimental

2.1. Synthesis

To prepare $Mn_xCo_{1-x}Fe_2O_4$ NPs, stoichiometric molar amounts of manganese nitrate [$Mn(NO_3)_2{\cdot}6H_2O$], cobalt nitrate [$Co(NO_3)_2{\cdot}6H_2O$] and ferric nitrate [$Fe(NO_3)_3{\cdot}9H_2O$] were each dissolved in 10 mL of distilled water to form a clear solution and mixed altogether. The mixture was stirred with a magnetic stirrer until the reactants were dissolved completely. During the stirring, 10 ml PEG-400 was added to the solution to serve as surfactant that covers NPs and prevents agglomeration. And then pH of the solution was adjusted to 11.5 by adding 2 M NaOH drop-by-drop. After continuous stirring at 400 rpm for an hour, a homogeneous solution could be obtained. The obtained solutions were put into the autoclaves up to two thirds of their total volume (50 mL). Lastly, the autoclaves were left in an oven at 180 °C for 24 h and then were allowed to cool to room temperature. The products were centrifuged and washed several times with de-ionized water, acetone and absolute ethanol. Then the samples were put again in an oven at 70 °C to dry. Taken solid phase samples were grinded in a mortar to make them powder. Obtained powders were used for all of the measurements.

2.2. Measurements

X-ray powder diffraction analysis was conducted on a Huber JSO-DEBYEFLEX 1001 Diffractometer (XRD) using CuK_α (operated at 40 kV and 35 mA). FT-IR transmission spectra were taken on Mattson Satellite Infrared Spectrometer from 4000 to 400 cm^{-1}.

Field Emission Scanning Electron Microscope (FE-SEM, JEOL 7001 FE with EDX) was used in order to investigate the nanostructure, morphology and elemental composition of the sample. Sample was coated with carbon prior to SEM analysis.

Magnetization measurements were performed by using a Quantum Design Vibrating sample magnetometer (QD-VSM). The sample was measured between ±50 kOe at room temperature and 50 K. ZFC (zero field cooling) and FC (field cooling) measurements were carried out at 1500 Oe and the blocking temperature was determined from the measurements.

3. Results and discussion

3.1. FT-IR spectroscopy

Fig. 1 exhibits the IR spectra of $Mn_xCo_{1-x}Fe_2O_4$ NPs. Two main metal–oxygen bands are generally observed in the IR spectra of all spinel structures. The one with the higher wave number, ν_1, is observed in the range of 500–600 cm^{-1},

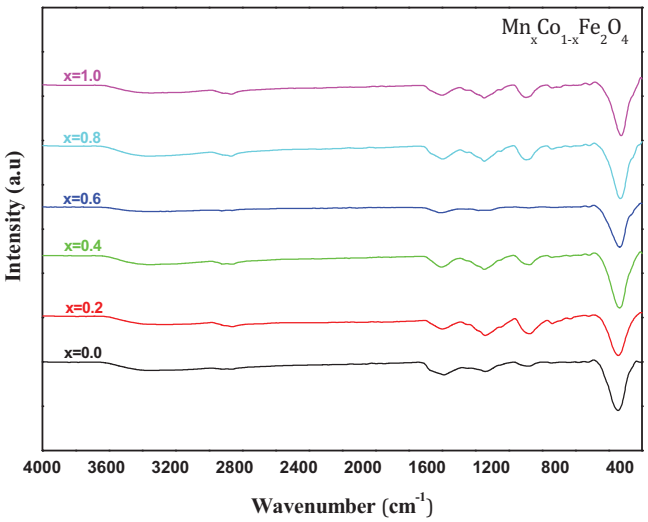

Fig. 1. FT-IR spectra of $Mn_xCo_{1-x}Fe_2O_4$ NPs.

Table 1
Data of obtained characteristic parameters for each composition at room temperature.

Composition	ν_1 (cm^{-1})	D_{XRD} (nm)	a (Å)	T_B (K)	H_c (Oe)	M_r (emu/g)	M_r/M_s	M_s (emu/g)	K_{eff} (erg/cm^3)
$CoFe_2O_4$	520.6	17.38	8.474	355	831.0	23.11	0.364	63.48	0.45×10^6
$Mn_{0.2}Co_{0.8}Fe_2O_4$	528.6	13.92	8.452	329	578.0	18.35	0.311	59.00	0.8×10^6
$Mn_{0.4}Co_{0.6}Fe_2O_4$	532.1	16.51	8.450	320	688.3	20.53	0.342	59.99	0.47×10^6
$Mn_{0.6}Co_{0.4}Fe_2O_4$	536.0	19.80	8.428	297	596.3	21.73	0.341	63.65	0.25×10^6
$Mn_{0.8}Co_{0.2}Fe_2O_4$	540.0	18.59	8.410	244	338.4	12.88	0.202	63.92	0.25×10^6
$MnFe_2O_4$	543.0	22.05	8.400	30	54.8	3.86	0.059	65.49	0.018×10^6

corresponds to intrinsic stretching vibrations of the metal at the tetrahedral site, $M_{tetra} \leftrightarrow O$. And the other one, ν_2, is usually observed in the range of 385–450 cm^{-1}, is attributed to octahedral-metal stretching, $M_{octa} \leftrightarrow O$ [24,25]. The stretching of the O–H bands can be seen around 1500 cm^{-1} and the bending of the O–H bands is around 3500 cm^{-1}. However, no clear peak due to metal ions at the octahedral site has been observed, which is predictable to occur below 400 cm^{-1}. Since our FTIR spectra ranges between 400 and 4000 cm^{-1} we could not observe, ν_2, which is attributed to octahedral-metal stretching, $M_{octa} \leftrightarrow O$. This may be due to the broadening of this peak attributed to very tiny particles of spinel ferrites [26].

When the Mn-substitution increases, characteristic band (ν_1) of spinel ferrites shifts to higher frequency region (see Table 1). This is because the atomic mass of manganese is lighter than that of cobalt. So metal–oxygen stretching frequency will be increased.

3.2. XRD analysis

XRD studies of products have proved the formation of single phase cubic spinel structure for all samples. The miller indices ($h\,k\,l$) help us to identify our sample. The $h\,k\,l$ indices of the samples are [1 1 1], [2 2 0], [3 1 1], [2 2 2], [4 0 0], [4 2 2], [5 1 1] and [4 4 0] as plotted in Fig. 2. These planes are indications of the presence of a mixed type cubic spinel structure. Mixed spinel ferrites ($x = 0.0, 0.2, 0.4, 0.6, 0.8, 1.0$) were checked with XRD cards of pure $CoFe_2O_4$ ($x = 0.0$) (JCPDS file no: 22-1086) and pure $MnFe_2O_4$ ($x = 1.0$) (JCPDS file no: 74-2403) [26]. Using XRD results, crystallite sizes were calculated by using Debye–Scherrer equation:

$$D_{XRD} = \frac{0.9\lambda}{\beta \cos\theta} \quad (1)$$

Here, D_{XRD} stands for crystallite size; λ is the wavelength of the radiation and β is the full width at half maximum (in radians) centered at 2θ of the most intense peak (in this case it is the peak of [3 1 1]) [27–29]. The calculated sizes of the particles vary in the range of 14–22 nm (see Table 1).

The lattice parameters have been computed using the d-spacing values and the respective ($h\,k\,l$) parameters from the classical formula given in Eq. (2).

$$a = \frac{\lambda}{2} \frac{[h^2 + k^2 + l^2]^{1/2}}{\sin\theta} \quad (2)$$

The lattice constant is affected by the cationic stoichiometry. The lattice parameters are found to decrease almost linearly by increasing Mn content. This is because the ionic radius of Mn^{2+} (0.66 Å) is smaller than the ionic radius of Co^{2+} (0.74 Å) [30]. The values of the lattice parameter exhibit an almost linear dependence, thus obeying Vegard's law [31] as shown in Fig. 3.

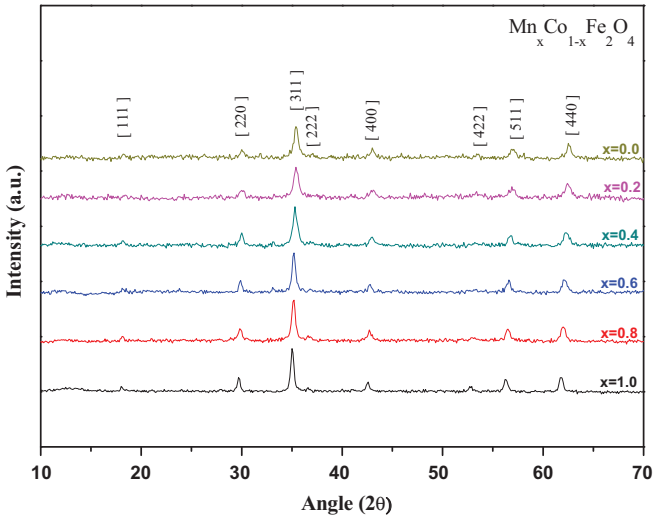

Fig. 2. XRD patterns for $Mn_xCo_{1-x}Fe_2O_4$ NPs.

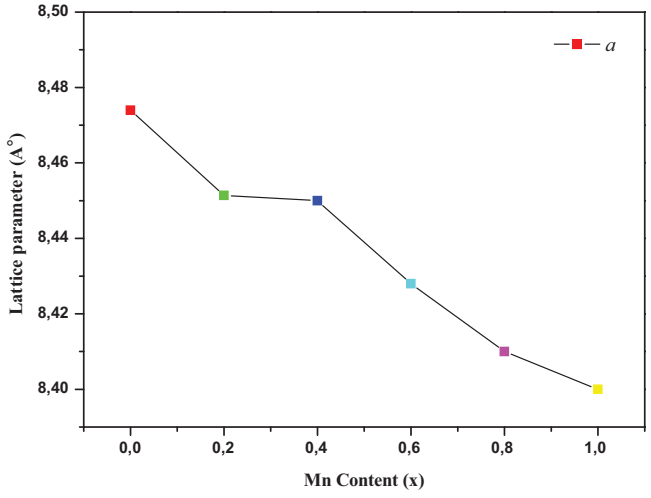

Fig. 3. Variation of lattice parameter (a) with composition.

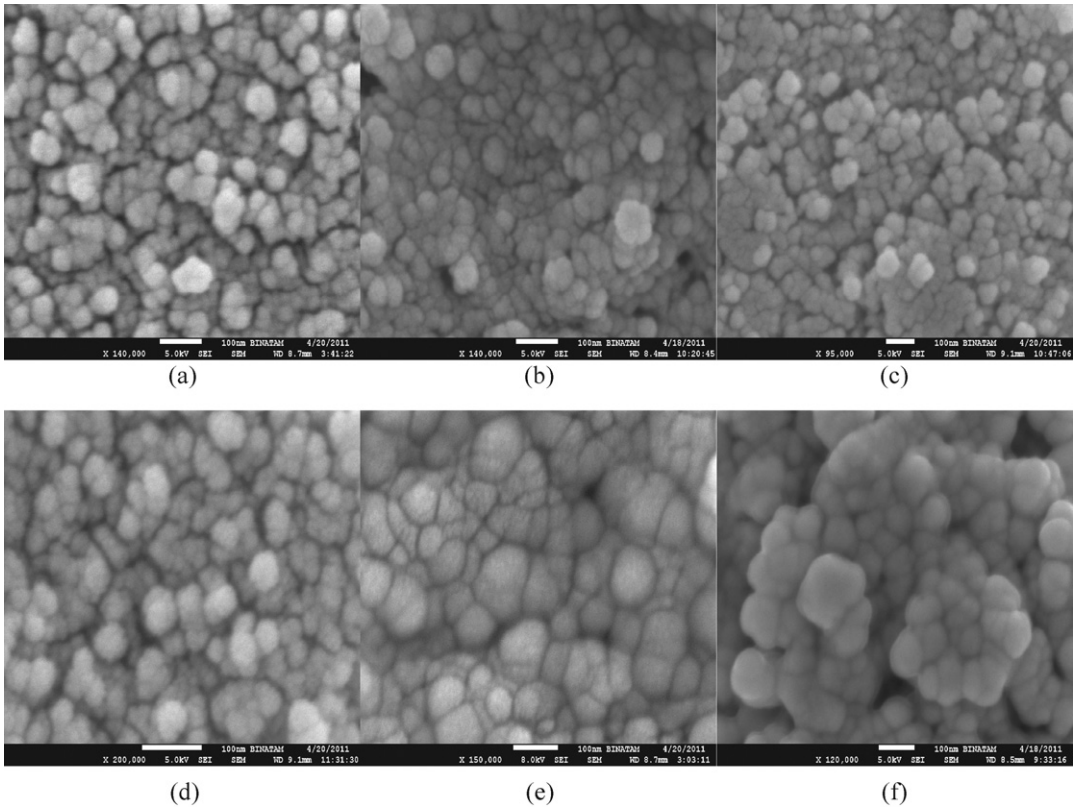

Fig. 4. SEM images of the $Mn_xCo_{1-x}Fe_2O_4$ NPs with $x = 0.0$ (a), $x = 0.2$ (b), $x = 0.4$ (c), $x = 0.6$ (d), $x = 0.8$ (e) and $x = 1.0$ (f).

3.3. SEM analysis

Fig. 4 shows the field emission scanning electron micrographs (FE-SEM) of $Mn_xCo_{1-x}Fe_2O_4$ NPs. SEM images indicate that the samples consist of spherical shaped NPs with the existence of soft agglomeration. They also reveal that smaller crystallites have sizes less than 100 nm (Fig. 4(a)–(f)). Nanoparticles are dense and distributed regularly on the whole area. In addition to this, although these smaller crystallites are so closely arranged together, a clear boundary between neighboring crystallites can yet be observed. The larger particle sizes of the NPs can be attributed the PEG coating which does not count in crystallite sizes since PEG is amorphous.

3.4. EDX spectroscopy

EDX (or EDS) measurement results comply with what is expected from the synthesis. In other words, mass ratios of chemical compositions are in agreement with the outcomes of the EDX spectra (see Fig. 5 and Table 2). Both ideal and experimental mass ratios for the sample $x = 0.2$ are given in Table 2 as an example. Since the NPs are covered with PEG, remaining % 15 of the experimental mass ratio belongs to PEG which is composed mainly of carbon atoms. The presence of C atoms may also be given to carbon-coating for SEM measurement which was applied prior to EDX measurement.

3.5. Magnetization studies

3.5.1. Variation of magnetization by applied magnetic field

Fig. 6 shows the isothermal hysteresis loops of the $Mn_xCo_{1-x}Fe_2O_4$ nanoparticles collected at some selected temperatures. The room-temperature magnetization curves display relatively higher M_s values between 59 and 65 emu/g. All M_s values are, however, somewhat lower than the bulk values (110 emu/g for $MnFe_2O_4$ and 93.9 emu/g for $CoFe_2O_4$). The obtained values of M_s for the as synthesized samples are slightly grater than those obtained by Shobana et al. [21] and Abdallah et al. [32] and less than those obtained by Carta et al. [33]. The M–H curve has an s-shape at lower fields and a linear part at higher fields. The hysteresis loops show essentially small coercivity, suggesting that improved coalescence of the crystallites in the nanostructures resulting increased magnetic coupling and higher magnetization. The magnetization properties such as, saturation magnetization (M_s), coercivity (H_c) and remanent magnetization (M_r) are all affected differently by Mn

Table 2
EDX results of $Mn_{0.2}Co_{0.8}Fe_2O_4$ NPs.

Element	Mass percentage (ideal)	Mass percentage (Exp.)
Mn	4.70	4.60
Co	20.16	18.04
Fe	47.77	42.64
O	27.37	20.06
Compound (total)	100.00	85.34

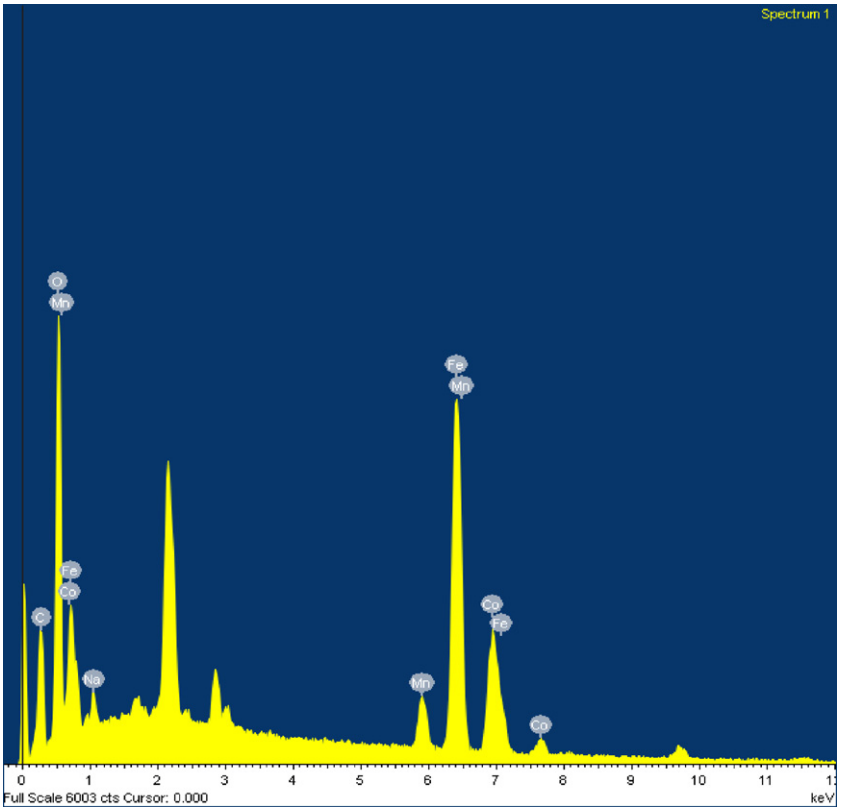

Fig. 5. EDX spectra of the $Mn_{0.2}Co_{0.8}Fe_2O_4$ NPs.

content. As the Mn content increase, the coercivity decreases and tends to be zero at the maximum Mn content. This suggests that the samples tend to show superparamagnetic behavior by the increase in Mn content. While the coercivity values are significantly reduced by Mn substitution, the changes in M_s are not dramatic.

M–H curves taken at 10 K indicate that all the samples have ferromagnetic behavior with different coercivity values. Since Co ions have more anisotropic behavior than Mn ions, the coercivity of the samples at 10 K are found to decrease by Mn doping. In addition, for such fine nanoparticles, surface effects are relatively dominant; therefore, the surface spins also contribute considerably to the observed magnetization.

From *M–H* curve, it can easily be seen that when Mn content is increased, the coercive field decreases because Mn is a soft magnetic material. Mn concentration also affects the saturation magnetization and remanent magnetization. It is known that magnetization is related with the magnitude of electron magnetic dipole moment. In this context, keeping in mind that Mn has 5 μ_B and Co has 3 μ_B as their magnetic dipole moments, as Mn content is increased, it is seen that saturation magnetization also increases as evidently seen in Fig. 6.

In the spinel structure the cations on different sublattices (A and B sites) have oppositely aligned magnetic moments according to the Néel's ferrimagnetic theory [34]. So the magnetic moment per formula unit in μ_B (Bohr magnetron) is as follows,

$$\eta B(x) = M_B(x) - M_A(x) \quad (3)$$

In Eq. (3), M_B and M_A are sub-lattice B's and sub-lattice A's magnetic moments in units of μ_B. The samples behave like superparamagnetic materials because the thermal fluctuation energy is bigger than magnetization energy. Therefore, there is too small coercive field.

3.5.2. *Variation of coercivity by composition and temperature*

Fig. 7 depicts the variation of the coercive fields with the temperature and Mn concentration. It can be clearly observed that the coercivity of the samples decrease by the increase in Mn content and temperature. This can be attributed to the much larger magnetocrystalline anisotropy characteristic of the cobalt ferrite. It is known that, in a randomly oriented ferromagnet the coercivity follows a non-monotonic function of temperature. At low temperatures the coercivity is large due to the scattering in direction of anisotropic field of particles (inhomogeneous broadening). As the temperature increases the tendency to make magnetic moment isotropic causes the coercivity to decrease [17,35].

Below the blocking temperature T_B the surface spins freeze and they freeze in the direction of DC-magnetic field. This yield an exchange coupling between the surface and core spins. This gives rise to a 'unidirectional' anisotropy with easy axis in the direction of the field. As a result, there is a sudden increase in the coercive field below T_B. The coercivity values at lowest temperature for $MnFe_2O_4$ and $CoFe_2O_4$ samples are higher than those of reported in literature for each ferrite in its bulk form, as

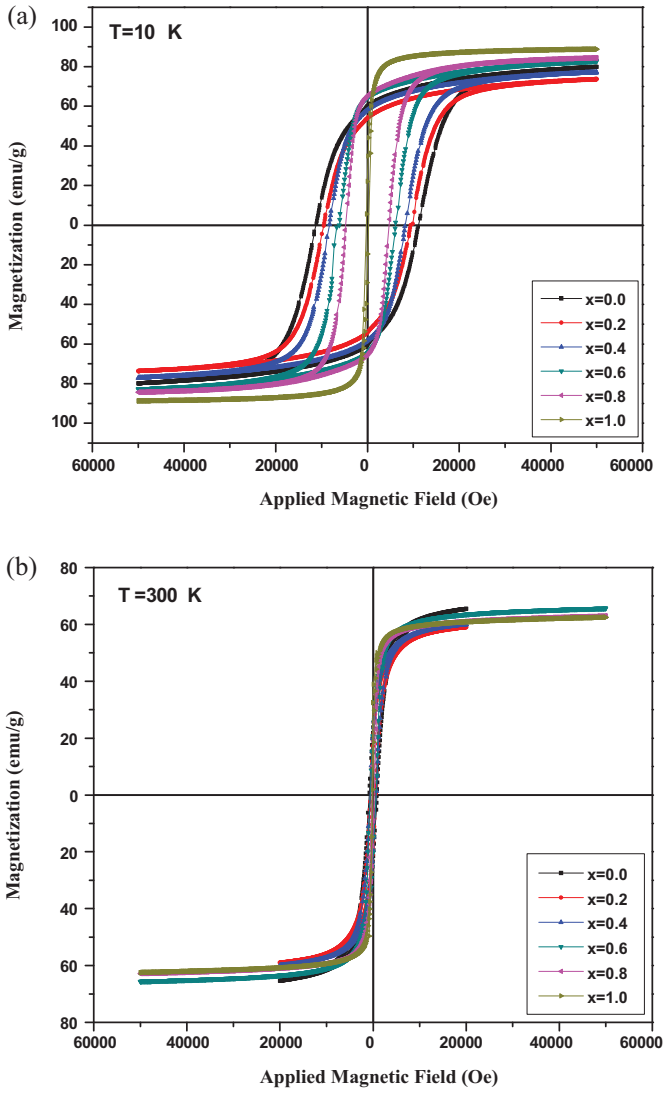

Fig. 6. *M–H* Curves of $Mn_xCo_{1-x}Fe_2O_4$ NPs measured at 10 K (a) and 300 K (b).

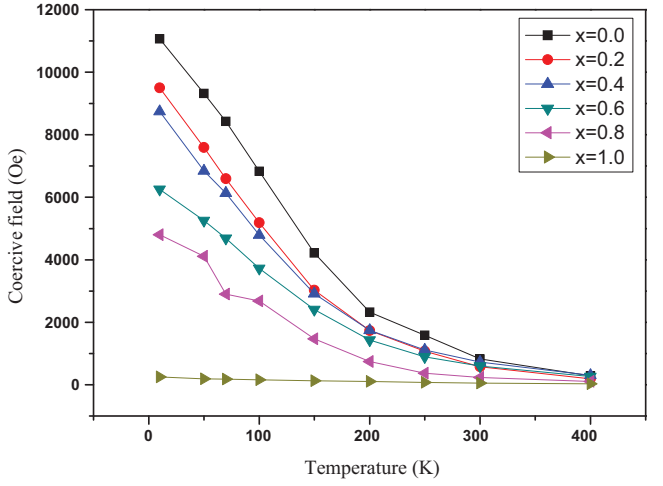

Fig. 7. Temperature variation of the coercivity for all samples.

expected for nanoparticles. But, they are smaller than the values obtained by Carta et al. [33].

3.5.3. Variation of magnetization by temperature

Fig. 8 shows the zero field cooling (ZFC) and field cooling (FC) curves of the samples measured in an applied magnetic field of 1500 Oe. For all curves ZFC and FC follows the same path at high temperature regime. The observed irreversibility is due to characteristic blocking-unblocking process of the particle magnetic moment when thermal energy is changed. By decreasing the temperature, the relaxation time of magnetic particle increases, below a characteristic temperature, called the blocking temperature (T_B), the particle moment appears blocked with respect to the time scale of the experiment. At T_B, the thermal energy k_BT (T is T_B and k_B is the Boltzmann's constant) equals the energy barrier for the magnetic moment reversal associated with the total anisotropy energy, $E_B = K_{eff}V$ where K_{eff} is the anisotropy energy density, which is proportional to the particle volume V. While decreasing temperature ZFC curve increases and reaches a maximum (cusp) at temperatures (T_B) above 240 K except for $MnFe_2O_4$, it suddenly decreases below T_B (see Fig. 8). The blocking temperature (T_B) is a characteristic magnetic phase transition temperature determined according to the maximum value of a ZFC curve. The blocking temperatures for all samples are given in Table 1. For all ZFC–FC graphs, above the blocking temperatures, the thermal fluctuation energy (k_BT) is larger than magnetic energy ($K_{eff}V$). And below T_B, magnetic energy is larger than the thermal fluctuation energy [17,36]. Above T_B, the single particle magnetic moment unblocks and the magnetization in the presence of a magnetic field reaches its thermal equilibrium. Since the magnetic moment of a single particle is much higher than that of an atom, the magnetic state at the temperatures higher than T_B is called as super-paramagnetic.

At the blocking temperature, it is usually assumed that

$$K_{eff}V = 25k_BT_B \quad (4)$$

K_{eff} contains all of the different contributions to the effective anisotropy given by the magnetocrystalline, shape, surface, and, stress magnetic anisotropies. Also, a further contribution to the effective anisotropy can be given by the presence of dipolar and/or exchange interactions among the nanoparticles [5,10,33]. By using Eq. (4), consider the particle mean size D for each sample as determined by Scherrer equation, K_{eff} values can roughly be determined. Obtained K_{eff} values for Mn doped $CoFe_2O_4$ nanoparticles are varying between 0.018×10^6 and 0.8×10^6 erg/cm^3 (see Table 1). K_{eff} values for manganese ferrite and cobalt ferrite are found to be 0.018×10^6 and 0.45×10^6 erg/cm^3, respectively. These values are smaller than those of reported bulk values (0.025×10^6 and 1.8×10^6 erg/cm^3) [33].

The large cusps in the *M–T* curves have also been observed for similar systems which were attributed to the interaction between the NPs in the samples [37–39] or grain growth effect as the samples were heated at high temperatures [37]. T_B is

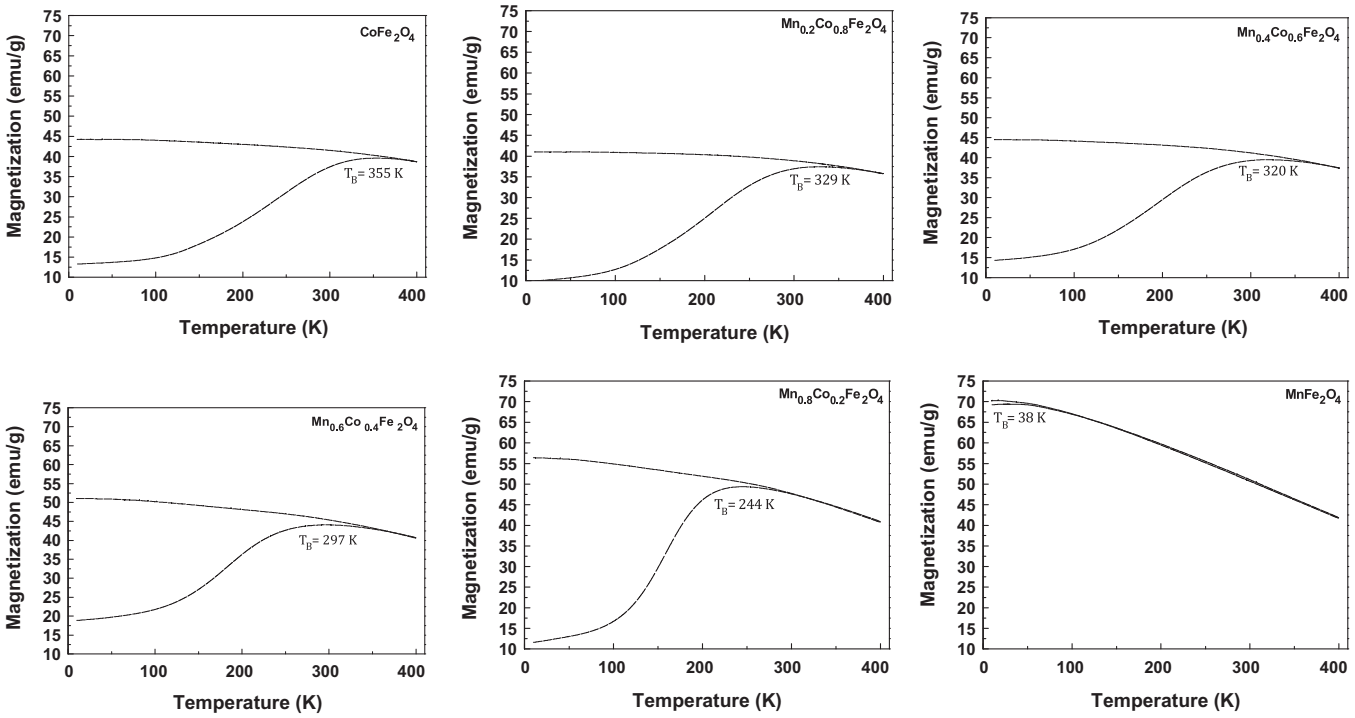

Fig. 8. Blocking temperatures for the $Mn_xCo_{1-x}Fe_2O_4$ nanoparticles.

determined by the intersection of the tangent line at the largest slope with the horizontal axis (see Fig. 8). In addition, T_B values of the samples are also found to decrease considerably with increasing the manganese content (see Fig. 9 and Table 1) which may be related to the lowering of the inter-sublattice exchange coupling between A and B sub-lattices. As reported previously for bulk ferrites, the exchange integral $J^A Fe^{3+}–^B Co^{2+}$ between Fe^{3+} ion in A lattice and Fe^{2+} in B lattice is larger than $J^A Fe^{3+}–^B Mn^{2+}$ between Fe^{3+} ion in A lattice and Mn^{2+} in B lattice [40,41].

The width of the peak in ZFC-curve is associated with particle size distribution [42]. A particle with a particular size has a certain blocking temperature. The wide peak observed in our samples indicates wide distribution of particle sizes. While the smaller particles behave as superparamagnetic, the larger particles behave as ferromagnetic. For an ensemble of magnetic nanoparticles with easy axis randomly distributed over entire space and with a certain size distribution, the total anisotropy energy barrier is distributed over a certain range. Therefore, since the blocking temperature is measured on the entire nanoparticles ensemble, it has to be considered as mean value [5,10,12,16,17,19]. The lower blocking temperature in the sample $x = 1.0$ relates with the superparamagnetic nature of manganese ferrite.

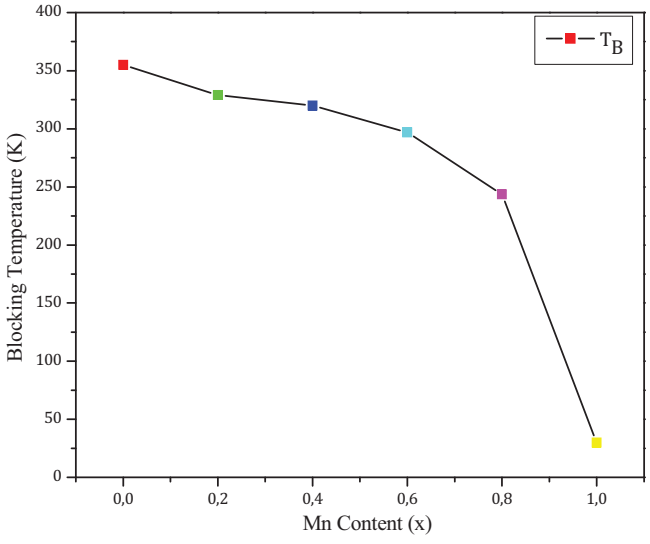

Fig. 9. Variation of blocking temperature, T_B, with Mn content, x.

As the NPs are cooled to a very low temperature in the presence of a magnetic field (FC), the magnetization direction of each particle is frozen in the field direction. While the ZFC magnetization is decreasing, FC magnetization is increasing by decreasing the temperature. Both curves separate and the separation between the ZFC and the FC curves gives an indication that there is a non-equilibrium magnetization below the separation temperature for the ZFC case, and represents the irreversibility temperature, T_{irr}. In general, T_{irr} represents the blocking temperature of particles with the highest energy barrier and T_{max} (T_B) is related to the average blocking temperature. The difference between T_{max} and T_{irr} corresponds to the width of the blocking temperature distribution [43,44]. Below the T_{irr}, the ZFC and FC curves significantly diverge and the sample is in the ferromagnetic state. The divergence in the ZFC–FC magnetization curves below T_B is attributed to the existence of magnetic anisotropy barriers [44].

Considering variations of T_B with composition, while the concentration of manganese is increased, the T_B is decreasing due to two possible explanations: One of them is particle size

effect which arises when size is decreased; it requires less energy to flip a small particle. Second possible explanation is magneto-crystalline anisotropy effect. Since Mn content intensifies in the samples, it is easier to flip Mn's spins from easy axis to hard axis than doing so with Co's spins [41].

3.5.4. Magnetization parameters

All data of the magnetization parameters are included in Table 1 and variation of these parameters with the Mn content is shown in Fig. 10. Looking at Fig. 10, when Mn content is increased; the slope of coercive field tends to decrease. This is because $MnFe_2O_4$ is a soft ferrite, which means that it has almost no coercivity and $CoFe_2O_4$ is a hard ferrite with large coercivity. Since coercivity is a measure of magneto-crystalline anisotropy, the increase of coercivity with Co content can be attributed to anisotropic property of Co ion [10,35]. Like coercive field variation, as the Mn content is increased, the slope of remanent magnetization is also decline (as plotted in Fig. 10 with open triangle line) because manganese ferrite has

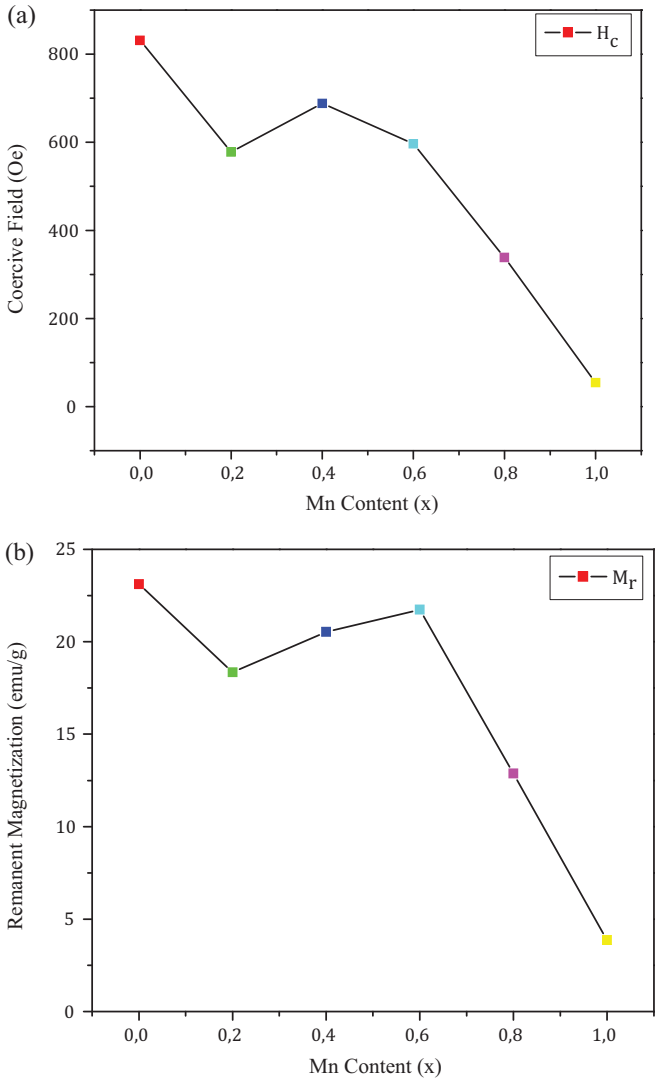

Fig. 10. Compositional variation of coercivity (a) and remanence (b) of $Mn_xCo_{1-x}Fe_2O_4$ nanoparticles.

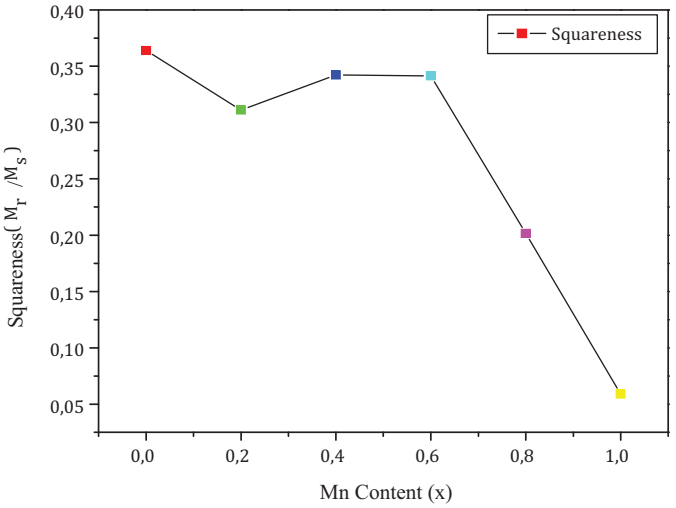

Fig. 11. Variation of squareness parameter with Mn content.

no remanence; again since it is a soft ferrite. So, the remanent magnetization comes from the cobalt ions present in the samples.

Fig. 11 depicts the compositional variation of the ratio of remnant magnetization (M_r) over saturation magnetization (M_s) at room temperature measurement. In other words, this ratio (M_r/M_s) is called squareness and is an important characteristic parameter for applications of ferromagnetic materials. While going from $CoFe_2O_4$ ($x = 0.0$) to $MnFe_2O_4$ ($x = 1.0$), this parameter reduces in general [34], mostly because of the fact that as the amount of Co content lessens, magnetic anisotropy of the samples decays.

As a comparison of literature, the parameters (see Table 1) of saturation magnetization (M_s), remanence (M_r) and coercivity (H_c) are all smaller than those found in a similar study of Mn–Co ferrites by Kambale et al. [45]. Additionally, greater values for M_s and H_c are found when compared to the study of Choi et al. [46]. Lastly, we found greater M_r and H_c values and lower M_s values than those reported by Msomi et al. [47]. It is also known that all these parameters are somehow dependent on particle size, shape, density, crystal defects and synthesis methods or conditions [48].

4. Conclusion

Manganese-substituted cobalt ferrite nanoparticles of $Mn_xCo_{1-x}Fe_2O_4$ have been prepared successfully by using surfactant (PEG)-assisted hydrothermal route. The method used allows us to synthesize spinel type structures with good crystallinity and reproducibility. The structural characterizations have revealed that Mn doped $CoFe_2O_4$ nanoparticles have a single spinel structure with sizes ranging between 14 and 22 nm. The size of the crystallites and lattice parameters decrease by Mn content due to smaller ionic size of manganese ions. VSM measurements have shown that the $Mn_xCo_{1-x}Fe_2O_4$ nanoparticles have ferromagnetic behavior (except $x = 1.0$) where the $MnFe_2O_4$ has superparamagnetic behavior at room temperature. The saturation magnetization of the sample

increases with the increase in Mn content and decrease by the temperature. The coercivity, effective anisotropy constant and the remnant magnetization a of the samples increase by the decrease in Mn content which are attributed to anisotropic nature of Co ions. At room temperature, the magnetic phase of the samples tends to be superparamagnetic by increasing Mn content.

Acknowledgement

This research was supported by Fatih University under grant no P50011001-2.

References

[1] T. Özkaya, A. Baykal, M.S. Toprak, Y. Köseoğlu, Z. Durmus, Reflux synthesis of Co_3O_4 nanoparticles and its magnetic characterization, J. Magn. Magn. Mater. 321 (2009) 2145–2149.
[2] A.R. Shyam, R. Dwivedi, V.S. Reddy, K.V.R. Chary, R. Prasad, Vapour phase methylation of pyridine with methanol over the $Zn_{1-x}Mn_xFe_2O_4$ ($x = 0$, 0.25, 0.50, 0.75 and 1) ferrite system, Green Chem. 4 (2002) 558–561.
[3] V.S. Reddy, A.R. Shyam, R. Dwivedi, R.K. Gupta, V.R. Chumbale, R. Prasad, Ortho-selective vapour phase methylation of phenol over nanocrystalline ferrospinels of varying Zn^{2+}/Mn^{2+} ionic composition, J. Chem. Technol. Biotechnol. 79 (2004) 1057–1064.
[4] Y. Cheng, Y. Zheng, Y. Wang, F. Bao, Y. Qin, Synthesis and magnetic properties of nickel ferrite nano-octahedra, J. Solid State Chem. 178 (2005) 2394–2397.
[5] Y. Köseoğlu, H. Kavas, Size and surface effects on magnetic properties of Fe_3O_4 nanoparticles, J. Nanosci. Nanotechnol. 8 (2008) 584–590.
[6] Y. Chen, J.E. Snyder, C.R. Schwichtenberg, K.W. Dennis, R.W. McCallum, D.C. Jiles, Metal-bonded Co-ferrite composites for magnetostrictive torque sensor applications, IEEE Trans. Magn. 35 (1999) 3652–3654.
[7] Y. Chen, J.E. Snyder, K.W. Dennis, R.W. McCallum, D.C. Jiles, Temperature dependence of the magneto-mechanical effect in metal-bonded cobalt ferrite composites under torsional strain, J. Appl. Phys. 87 (2000) 5798–5800.
[8] J.G. Na, T.D. Lee, S.J. Park, Effects of cation distribution on the magnetic and electrical properties of cobalt ferrite, IEEE Trans. Magn. 28 (1992) 2433–2435.
[9] C.C.H. Lo, A.P. Ring, J.E. Snyder, D.C. Jiles, Improvement of magnetomechanical properties of cobalt ferrite by magnetic annealing, IEEE Trans. Magn. 41 (2005) 3676–3678.
[10] Y. Köseoğlu, M. Bay, M. Tan, A. Baykal, H. Sözeri, R. Topkaya, N. Akdoğan, Magnetic and dielectric properties of $Mn_{0.2}N_{i0.8}Fe_2O_4$ nanoparticles synthesized by PEG-assisted hydrothermal method, J. Nanopart. Res. 13 (2011) 2235–2244.
[11] N. Kasapoğlu, A. Baykal, Y. Köseoğlu, M.S. Toprak, Microwave-assisted combustion synthesis of $CoFe_2O_4$ with urea and its magnetic characterization, Scripta Mater. 57 (2007) 441–444.
[12] Y. Köseoğlu, H. Kavas, B. Aktaş, Surface effects on magnetic properties of superparamagnetic magnetite nanoparticles, Phys. Status Solidi (a) 203 (2006) 1595–1601.
[13] R.D. McMichael, R.D. Shull, L.J. Swartzendruber, L.H. Bennett, R.E. Watson, Magnetocaloric effect in superparamagnets, J. Magn. Magn. Mater. 111 (1992) 29–33.
[14] A. Ghasemi, A. Hossienpour, A. Morisako, A. Saatchi, M. Salehi, Electromagnetic properties and microwave absorbing characteristics of doped barium hexaferrite, J. Magn. Magn. Mater. 302 (2006) 429–435.
[15] Y. Sahoo, M. Cheon, S. Wang, H. Luo, E.P. Furlani, P.N. Prasad, Field-directed self-assembly of magnetic nanoparticles, J. Phys. Chem. B 108 (2004) 3380–3383.
[16] R.H. Kodama, A.E. Berkowitz, E.J. McNiff Jr., S. Foner, Surface spin disorder in $NiFe_2O_4$ nanoparticles, Phys. Rev. Lett. 77 (1996) 394–397.
[17] Y. Köseoğlu, A. Baykal, F. Gözüak, H. Kavas, Structural and magnetic properties of $Co_xZn_{1-x}Fe_2O_4$ nanocrystals synthesized by microwave method, Polyhedron 28 (2009) 2887–2892.
[18] J. Ding, P.G. McCormick, R. Street, Magnetic properties of mechanically alloyed $CoFe_2O_4$, Solid State Commun. 95 (1995) 31–33.
[19] J.M.D. Coey, Noncollinear spin arrangement in ultrafine ferrimagnetic crystallites, Phys. Rev. Lett. 27 (1971) 1140–1142.
[20] W.S. Cho, M. Cho, J. Jeong, M. Choi, H.Y. Cho, B.S. Han, S.H. Kim, H.O. Kim, Y.T. Lim, B.H. Chung, J. Jeong, Acute toxicity and pharmacokinetics of 13 nm-sized PEG-coated gold nanoparticles, Toxicol. Appl. Pharmacol. 236 (2009) 16–24.
[21] M.K. Shobana, S. Sankar, Characterization of sol–gel-prepared nanoferrites, J. Magn. Magn. Mater. 321 (2009) 599–601.
[22] A. Jozefczak, A. Skumiel, Ultrasonic investigation of magnetic nanoparticles suspension with PEG biocompatible coating, J. Magn. Magn. Mater. 323 (2011) 1509–1516.
[23] M. Tan, Y. Köseoglu, F. Alan, E. Şentürk, Overlapping large polaron tunneling conductivity and giant dielectric constant in $Ni_{0.5}Zn_{0.5}Fe_{1.5}Cr_{0.5}O_4$ nanoparticles (NPs), J. Alloys Compd. 509 (2011) 9399–9405.
[24] S. Hafner, The absorption of some metal oxides with spinel structure, Z. Kristallogr. 115 (1961) 331–358.
[25] R.D. Waldron, Infrared spectra of ferrites, Phys. Rev. 99 (1955) 1727–1735.
[26] J. Azadmanjiri, Structural and electromagnetic properties of Ni–Zn ferrites prepared by sol-gel combustion method, Mater. Chem. Phys. 109 (2008) 109–112.
[27] U. König, G. Chol, X-ray and neutron diffraction in ferrites of $Mn_xZn_{1-x}Fe_2O_4$ type, J. Appl. Crystallogr. 1 (1968) 124–126.
[28] K.P. Chae, J.G. Lee, H.S. Kweon, Y.B. Lee, The crystallographic, magnetic properties of Al, Ti doped $CoFe_2O_4$ powders grown by sol–gel method, J. Magn. Magn. Mater. 283 (2004) 103–108.
[29] N. Gupta, A. Verma, S.C. Kashyap, D.C. Dube, Microstructural, dielectric and magnetic behavior of spin-deposited nanocrystalline nickel–zinc ferrite thin films for microwave applications, J. Magn. Magn. Mater. 308 (2007) 137–142.
[30] J. Smith, H.P.J. Wijn, Ferrites: Physical Properties of Ferromagnetic Oxides in Relation to Their Technical Applications, Wiley, New York, 1959.
[31] M.A. Gabal, S.S. Ata-Allah, Effect of diamagnetic substitution on the structural, electrical and magnetic properties of $CoFe_2O_4$, Mater. Chem. Phys. 85 (2004) 104–112.
[32] H.M.I. Abdallah, T., Moyo, J.Z. Msomi, The effect of annealing temperature on the magnetic properties of $Mn_xCo_{1-x}Fe_2O_4$ ferrites nanoparticles, J. Supercond. Nov. Magn., doi:10.1007/s10948-011-1231-4.
[33] D. Carta, M.F. Casula, A. Falqui, D. Loche, G. Mountjoy, C. Sangregorio, A. Corrias, A. Structural, Magnetic investigation of the inversion degree in ferrite nanocrystals MFe_2O_4 (M = Mn, Co, Ni), J. Phys. Chem. C 113 (2009) 8606–8615.
[34] L. Néel, Aimantation à saturation des ferrites mixtes de nickel et de zinc, C. R. Acad. Sci. Paris 230 (1950) 375–377.
[35] M. Sertkol, Y. Köseoğlu, A. Baykal, H. Kavas, M.S. Toprak, Synthesis and magnetic characterization of $Zn_{0.7}Ni_{0.3}Fe_2O_4$ nanoparticles via microwave-assisted combustion route, J. Magn. Magn. Mater. 322 (2010) 866–871.
[36] T. Özkaya, M.S. Toprak, A. Baykal, H. Kavas, Y. Köseoğlu, B. Aktaş, Synthesis of Fe_3O_4 nanoparticles at 100 °C and its magnetic characterization, J. Alloys Compd. 472 (2009) 18–23.
[37] J.P. Chen, C.M. Sorensen, K.J. Klabunde, G.C. Hadjipanayis, E. Devlin, A. Kostikas, Size-dependent magnetic properties of $MnFe_2O_4$ fine particles synthesized by coprecipitation, Phys. Rev. B 54 (1996) 9288–9296.
[38] S. Morup, F. Bodker, P.V. Hendriksen, S. Linderoth, Spin-glass-like ordering of the magnetic moments of interacting nanosized maghemite particles, Phys. Rev. B 52 (1995) 287–294.
[39] J.P. Bouchaud, P.G. Zérah, Dipolar ferromagnetism: a Monte Carlo study, Phys. Rev. B 47 (1993) 9095–9097.
[40] W. Wolski, E. Wolska, J. Kaczmarek, P. Piszora, Formation of manganese ferrite by modified hydrothermal method, Phys. Status Solidi (a) 152 (1995) K19–K22.

[41] B.D. Cullity, C.D. Graham, Introduction to Magnetic Materials, Wiley-IEEE Press, 2009.
[42] A. Slawska-Waniewska, P. Didukh, J.M. Greneche, P.C. Fannin, Mössbauer and magnetisation studies of $CoFe_2O_4$ particles in a magnetic fluid, J. Magn. Magn. Mater. 215-216 (2000) 227–230.
[43] M. Sertkol, Y. Köseoğlu, A. Baykal, H. Kavas, A.C. Başaran, Synthesis and magnetic characterization of $Zn_{0.6}Ni_{0.4}Fe_2O_4$ nanoparticles via a polyethylene glycol-assisted hydrothermal route, J. Magn. Magn. Mater. 321 (2009) 157–162.
[44] H. Nathani, R.D.K. Misra, Surface effects on the magnetic behavior of nanocrystalline nickel ferrites and nickel ferrite–polymer nanocomposites, Mater. Sci. Eng. B 113 (2004) 228–235.
[45] R.C. Kambale, P.A. Shaikh, C.H. Bhosale, K.Y. Rajpure, Y.D. Kolekar, The effect of Mn substitution on the magnetic and dielectric properties of cobalt ferrite synthesized by an autocombustion route, Smart Mater. Struct. 18 (2009) 115028.
[46] H.N. Choi, K.S. Baek, S.W. Hyun, I.B. Shim, C.S. Kim, A study of Co substituted Mn–ferrite, $Mn_{1-x}Co_xFe_2O_4$ ($x = 0.0$, 0.5, 1.0), IEEE Trans. Magn. 45 (2009) 2554–2556.
[47] J.Z. Msomi, H.M.I. Abdallah, T. Moyo, A. Lancok, Structural and magnetic properties of $Mn_xCo_{1-x}Fe_2O_4$ ferrite nanoparticles, J. Magn. Magn. Mater. 323 (2011) 471–474.
[48] M.K. Shobana, S. Sankara, V. Rajendran, Characterization of $Co_{0.5}Mn_{0.5}$-Fe_2O_4 nanoparticles, Mater. Chem. Phys. 113 (2009) 10–13.